RESEARCH ARTICLE

StimFit—A Data-Driven Algorithm for Automated Deep Brain Stimulation Programming

Jan Roediger,[1,2*] Till A. Dembek, MD,[3] Gregor Wenzel, MD,[1] Konstantin Butenko, MS,[4] Andrea A. Kühn, MD,[1,5,6,7] and Andreas Horn, MD, PhD[1]

[1]*Movement Disorder and Neuromodulation Unit, Department of Neurology, Charité University Medicine Berlin, Charitéplatz 1, Berlin, 10117, Germany*
[2]*Einstein Center for Neurosciences Berlin, Charité University Medicine Berlin, Charitéplatz 1, Berlin, 10117, Germany*
[3]*Department of Neurology, Faculty of Medicine, University of Cologne, Cologne, Germany*
[4]*Institute of General Electrical Engineering, University of Rostock, Rostock, Germany*
[5]*Berlin School of Mind and Brain, Charité University Medicine, Berlin, Germany*
[6]*NeuroCure Clinical Research Centre, Charité University Medicine, Berlin, Germany*
[7]*DZNE, German Center for Degenerative Diseases, Berlin, Germany*

ABSTRACT: Background: Finding the optimal deep brain stimulation (DBS) parameters from a multitude of possible combinations by trial and error is time consuming and requires highly trained medical personnel.
Objective: We developed an automated algorithm to identify optimal stimulation settings in Parkinson's disease (PD) patients treated with subthalamic nucleus (STN) DBS based on imaging-derived metrics.
Methods: Electrode locations and monopolar review data of 612 stimulation settings acquired from 31 PD patients were used to train a predictive model for therapeutic and adverse stimulation effects. Model performance was then evaluated within the training cohort using cross-validation and on an independent cohort of 19 patients. We inverted the model by applying a brute-force approach to determine the optimal stimulation sites in the target region. Finally, an optimization algorithm was established to identify optimal stimulation parameters. Suggested stimulation parameters were compared to the ones applied in clinical practice.
Results: Predicted motor outcome correlated with observed outcome ($R = 0.57$, $P < 10^{-10}$) across patients within the training cohort. In the test cohort, the model explained 28% of the variance in motor outcome differences between settings. The stimulation site for maximum motor improvement was located at the dorsolateral border of the STN. When compared to two empirical settings, model-based suggestions more closely matched the setting with superior motor improvement.
Conclusion: We developed and validated a data-driven model that can suggest stimulation parameters leading to optimal motor improvement while minimizing the risk of stimulation-induced side effects. This approach might provide guidance for DBS programming in the future. © 2021 The Authors. *Movement Disorders* published by Wiley Periodicals LLC on behalf of International Parkinson and Movement Disorder Society

Key Words: subthalamic nucleus-deep brain stimulation; image-guided DBS; DBS programming; DBS sweet spot

***Correspondence to:** Jan Roediger, Movement Disorders and Neuromodulation Unit, Department of Neurology, Charité University Medicine, Charitéplatz 1, Berlin 10117, Germany; E-mail: jan.roediger@charite.de

Andrea A. Kühn and Andreas Horn contributed equally to this article.

Relevant conflicts of interest/financial disclosures: J.R., T.A.D., G.W., and K.B. have nothing to disclose. A.A.K. declares that she is on the advisory board of Boston Scientific and Medtronic and has received honoraria from Boston Scientific, Medtronic, Zambon, and Stadapharm. A.H. has received grants from the German Research Council.

Funding agencies: This study was funded by the Deutsche Forschungsgemeinschaft (DFG, German Research Foundation)—project ID 4247788381-TRR 295 grant and under Germany's Excellence Strategy—EXC-2049-390688087. J.R. is a fellow of the Berlin Einstein Center for Neurosciences PhD program. T.A.D. was supported by the Cologne Clinician Scientist Program (CCSP)/Faculty of Medicine/University of Cologne. This study was funded by the German Research Foundation (DFG, FI 773/15-1).

Received: 11 August 2021; **Revised:** 7 October 2021; **Accepted:** 4 November 2021

Published online 27 November 2021 in Wiley Online Library (wileyonlinelibrary.com). DOI: 10.1002/mds.28878

Deep brain stimulation (DBS) targeted at the subthalamic nucleus (STN) is highly efficacious in improving motor symptoms in Parkinson's disease (PD).[1] Current devices allow to adapt stimulation parameters to optimize therapeutic benefit according to patients' individual electrode placement and anatomy. However, in clinical practice, DBS programming currently follows a trial-and-error basis without deliberate guidance from these factors. In addition, the vast amount of parameter combinations, especially with octopolar DBS leads, cannot be tested individually in clinical routine. Even testing an informed subset of parameter combinations is tiring for both patient and medical personnel.

A clear relation between outcomes and one of the aforementioned factors—electrode placement—has been achieved over recent years,[2-7] namely, multiple studies concluded optimal stimulation sites to be localized at the dorsolateral border of the STN—at least when the aim was to explain variance across all symptoms covered by the motor part of the Unified Parkinson's Disease Rating Scale (UPDRS).[8-11] Symptom-specific stimulation sites have been suggested[8,12,13] but have not reached consensus across studies. Among these, more dorsally situated stimulation sites for optimal tremor reduction seem to be a robust finding.

Going one step further, first approaches aimed at creating automated programming based on DBS electrode localizations.[14-19] In a sense, these current approaches could be considered as a "model inversion" of optimal stimulation sites, that is, to derive stimulation settings that maximally engage predefined sweet-spot locations.

Such guided DBS programming has become more important by the introduction of eight-contact directional electrode designs.[20] These devices allow to distribute current in 1% steps across eight contacts, leading to an overwhelming number of $\sim 10^{10}$ possibilities of cathodal current distribution (even excluding bipolar settings). Adding additional contacts, such as 16 contact electrodes that are currently in clinical testing or 32 contact electrodes,[21] aiming to widen the therapeutic window will lead to an exponential increase in combinatorial possibilities (16 contacts: $\sim 10^{18}$, 32 contacts: $\sim 10^{30}$). In combination with other DBS parameters such as frequency and pulse width, exhaustively exploring the possibilities by clinical trial and error becomes an impossible endeavor, increasing the risk of selecting a suboptimal setting. At such a level, (semi-)automated programming strategies will become indispensable. Reducing the number of settings that need to be tested based on algorithmic pre-suggestions might therefore not only improve clinical benefit today but also facilitate future technological progress.

Currently, axonal activation models are considered state of the art. These models aim at solving the relationship between anatomical properties, electrode localization, applied electrical current, and subsequent firing of action potentials by axons of passage. Potential limitations of these models include that they require (1) exact anatomical definitions of pathways—which have shown to greatly impact fiber activation but simultaneously challenging if impossible to derive in a patient-specific manner,[22-25] and (2) a multitude of assumptions about the bioelectrical properties of the tissue. These include fiber diameters and myelination, degree of arborization, heterogeneity and anisotropy of tissue conductivity, and specific properties of the electrode tissue interface, including the encapsulation and the electrical double layer. Although some of them and similar parameters have been derived from animal studies,[26] their exact values remain unknown in individual patients.[27-29] Finally, action potential initiation is likely not the only relevant mechanism of action in DBS. Modulation of glial cells and intracellular cascades, transmitter depletion, and effects on complex network dynamics might contribute to therapeutic and/or unwanted effects.[30] Subsequently, alternative approaches that are slightly more naive to the biophysical models could potentially prove more robust toward a priori assumptions and therefore be considered to capture and predict DBS effects.

In the present study, a less-mechanistic approach was chosen, which is free from *biological* assumptions but still makes limited *physical* assumptions (eg, conductance of tissue). This model was integrated in a pipeline that is able to suggest optimal contacts and stimulation amplitudes in PD patients treated with STN-DBS. In the first step, we developed a novel approach capable of predicting motor improvements and side-effect probabilities based on the properties of the electric field (E-field) in the target region by harnessing a voxel-wise ensemble voting system. The model was trained and cross-validated on a large sample of standardized monopolar review data.[13,31] In the second step, its performance was tested on an independent cohort from a different center,[32] and optimal stimulation targets ("sweet spots") were identified. Finally, to derive at automatic suggestions of optimal DBS settings, we implemented an optimization algorithm that could consider motor improvements and side effects in parallel. Differences between automated and clinical settings in the test cohort were quantified to assess whether automated settings could have potentially led to superior clinical outcome.

Patients and Methods

Training Data Set

We included 31 patients who underwent bilateral STN-DBS at the University Hospital Cologne.[13,31] In brief, all patients underwent extended monopolar reviews after overnight withdrawal of dopaminergic medication. Data were obtained from both electrodes in 15 and unilaterally in 16 patients resulting in 46 electrodes (25 Medtronic 3389, 20 Boston Scientific Cartesia Directional, and 1 Boston Scientific linear eight contact). Single contacts were interrogated by increasing stimulation amplitudes in 1-mA steps to

a maximum of 5 mA or until nontransient side effects occurred. At each step rigidity, tremor, and akinesia were rated according to items 20 to 23 and 25 of the UPDRS, Part III. In this way 14 ± 5 settings were evaluated per electrode resulting in 612 settings. Stimulation frequency and pulse width were set at 130 Hz and 60 μs during the interrogation. Motor improvement was reported as relative change of the summed UPDRS items compared to baseline.

Test Data Set

The test data set consisted of 19 additional PD patients who underwent bilateral STN-DBS at Charité—Universitätsmedizin Berlin.[32] Clinical data were prospectively acquired within the scope of a study that investigated the effects of algorithm-guided DBS programming based on kinematic feedback. In this sample, two stimulation settings and corresponding clinical improvements were available, resulting from a prospective study in which the effectiveness of algorithm-guided programming based on kinematic feedback was compared to standard-of-care settings in a double-blind crossover design. In detail, wearable finger sensors were used to iteratively explore different stimulation settings based on motor performance until convergence to an optimal algorithm-based setting. UPDRS, Part III, scores were then evaluated by the same rater (G.W.) for both standard clinical and algorithm-based settings (further labeled as settings 1 and 2) in a double-blind crossover design and after a sufficient wash-in period.

Electrode Localization

Electrodes were reconstructed and normalized into the Montreal Neurological Institute (MNI) space (2009b, nonlinear, asymmetric) following the updated (v.2) default pipeline implemented in the Lead-DBS toolbox (www.lead-dbs.org[33,34]). Briefly, linear registrations between preoperative magnetic resonance imaging and postoperative computed tomography (CT) scans were performed using Advanced Normalization Tools (ANTs; http://stnava.github.io/ANTs/[35]). Normalization to MNI space was carried out using a multispectral implementation of the ANT symmetric diffeomorphic registration approach. PaCER and DiODe algorithms were used to reconstruct electrode locations and rotation postoperative CT imaging.[36,37] Left hemispheric electrodes were nonlinearly flipped to the right hemisphere. All steps were meticulously inspected and manually refined, if needed, to ensure maximal precision of lead localizations.

E-Field Simulation

A volume conductor mesh was constructed in template space using the tetrahedral mesh generator "TetGen" as included in Lead-DBS.[34,38,39] Conductivity (κ) values were assigned to each tetrahedral element as contact material ($\kappa = 10^8$ S/m), insulator ($\kappa = 10^{-16}$ S/m), or neural tissue ($\kappa = 0.2$ S/m). E-fields were then estimated by determining the static formulation of Laplace's equation using the finite element method on a discretized domain represented by the three-compartment mesh. This was performed using an adaptation of the FieldTrip-SimBio pipeline as implemented within Lead-DBS.[40,41] Analogous to the approach recently published by Baniasadi et al, computational demands were vastly reduced by avoiding FEM simulations for changes in amplitudes across settings but instead exploiting the linearity of Laplace's equation.[42] In short, an E-field template was generated once for each contact based on 1-mA cathodal stimulations. Scalar multiplication or superposition of these templates then allowed for simulating different stimulation amplitudes or multicathode configurations, respectively, without the need for computationally expensive FEM simulations.

Vector-Field Model

The novel approach outlined in this section was developed to predict DBS outcome based on the shape and magnitude of the E-field in the vicinity of the electrode (Fig. 1 graphically summarizes the following paragraph). E-field vectors were resampled on an isometric grid of 125,000 voxels of 0.8-mm size. Each voxel was further radially divided into 26 cone-shaped spherical sectors (together representing a sphere). Depending on its directionality, an E-field vector present at each voxel would fall into one of these sectors. Sectorizing therefore allowed storing information about the shape of the E-field. Next, in a mass-univariate attempt, generalized linear mixed-effects models were created for each sector and fit to clinical outcomes based on the magnitudes of the E-field vectors. Sectors that contained fewer than 30 data points were excluded. Because training data were based on monopolar reviews, they contained repeated measures for each electrode. To account for this, electrode IDs were included in the model as a random effect.

Whereas linear models were used to describe the relationship between the magnitude of the E-field and motor improvement, side-effect occurrence was modeled as a binary outcome using logistic regression.

Using data from the test cohort, valid models were determined iteratively, and a probability density function describing the probability distributions of predicted motor improvements and side-effect probabilities at each of the 125,000 voxels was calculated. Finally, these predictions were combined accounting for their individual accuracies by averaging their probability density functions to obtain an overall probability distribution. For more details on the vector-field model, we refer the reader to Appendix S1.

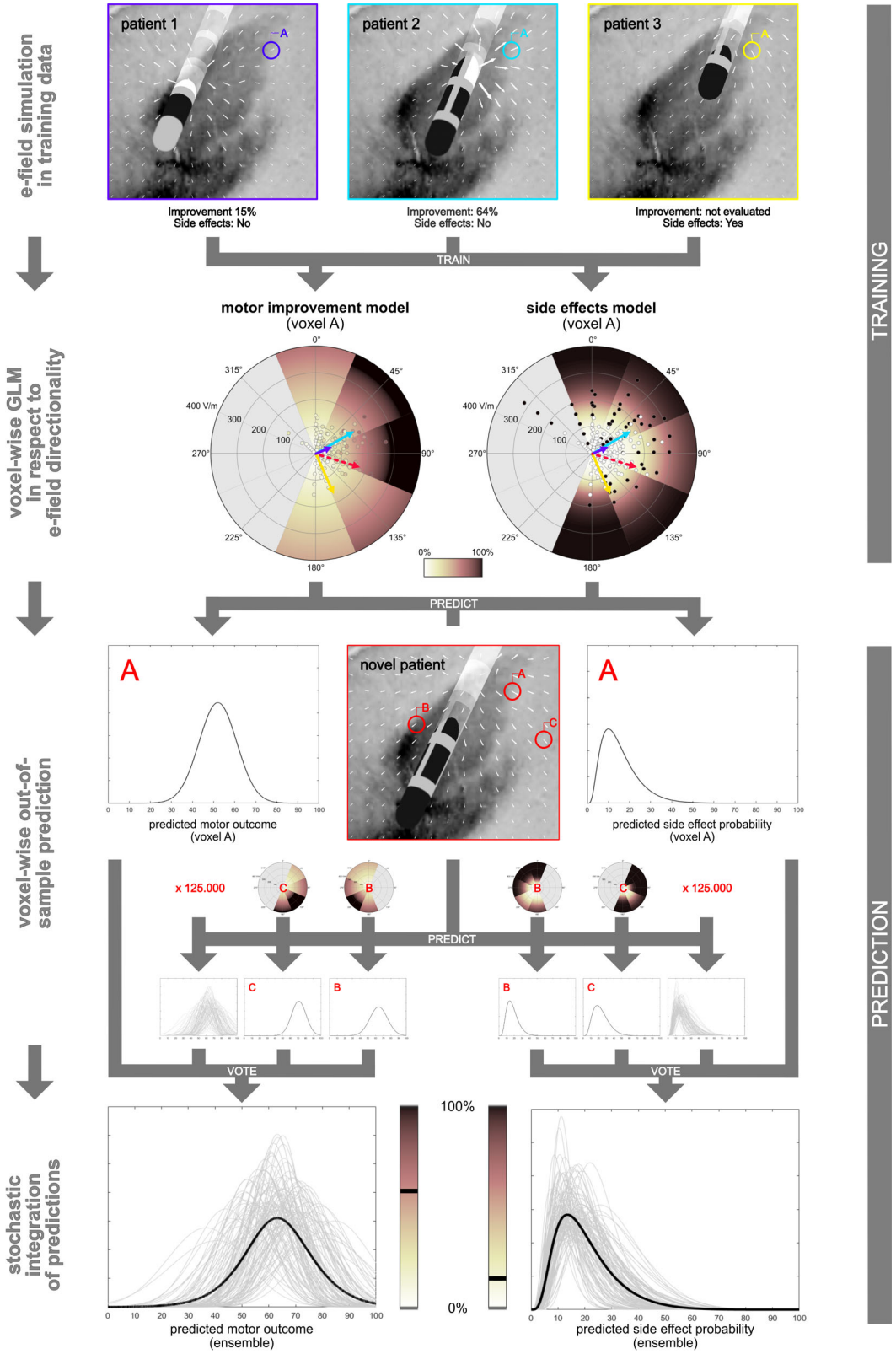

FIG. 1. Vector-field model. First row: simulation of E-fields generated by stimulation settings of patients 1, 2, and 3. Second row: motor outcome and side-effect models of voxel A are represented as polar plots that were radially divided into sectors. Magnitudes and clinical outcome of all vectors within one sector were used to train a generalized-mixed-effects model. Vectors of example patients 1 to 3 are plotted in purple, turquoise, and yellow. Sectors are colored according to the predicted clinical outcome in respect to vector magnitudes. Third row: the E-field of an out-of-sample patient is shown in the central panel framed in red. The vector of voxel A is shown in the polar plot as a dashed red arrow pointing toward the 90° sector. The predicted probability density functions of voxel A for motor and side effects are shown on the left and right, respectively. Fourth row: exemplary models of voxels B and C are shown together with their predicted solutions for the out-of-sample patient. Stochastic integration of all 125,000 voxel-wise predictions was carried out by averaging probability density functions, and their maxima were treated as final solutions. [Color figure can be viewed at wileyonlinelibrary.com]

Model Validation

Model performance within the training cohort was assessed using a fourfold cross-validation scheme. In detail, vector-field models were trained four times after dividing the training data into four random sets of approximately equal size. In each iteration, the model was trained on three sets to cross-predict motor outcomes and side-effect probabilities in the remaining set. Finally, model performance was evaluated by calculating the Pearson's correlation coefficient between observed and predicted motor improvement. Model performance regarding side effects was quantified by calculating the area under the receiver operating characteristic (ROC) curve. In addition, medians and interquartile ranges (IQRs) of predicted side-effect probabilities between settings with and without side-effect occurrence were obtained.

After model validation within the training sample, its predictive utility was further assessed in the independent test cohort. Performance was quantified by the Pearson correlation coefficient between predicted and observed differences in motor outcomes between the two settings. Here, performance of the side-effect arm of the model could not be evaluated because the test cohort constituted long-term DBS effects in which none of the settings induced permanent side effects.

Calculating an Optimal Stimulation Target

Exploiting the model to predict outcomes at arbitrary stimulation sites made it possible to estimate an optimal stimulation target (*sweet spot*). Here, we repeatedly simulated stimulations at each of the aforementioned 125,000 points in MNI space (corresponding to and surrounding the STN target region). At each point, 2 mA was applied on a circular contact, and predicted motor outcomes and side-effect probabilities were obtained and visualized. In a subsequent analysis, vector models were recalculated separately for tremor (UPDRS items 20 and 21) and akinetic-rigid symptoms (UPDRS items 22, 23, and 25). Here, symptom-specific sweet spots were obtained for both models following the same approach.

Nonlinear Optimization

Thus far, a novel data-driven approach that allowed to predict clinical effects of DBS settings based on the properties of the E-field in the subthalamic region had been developed and validated. However, these models would not result in actual optimal stimulation parameters that could maximally engage the optimal stimulation site (and avoid inducing side effects).

To do so, we implemented a solver based on the interior-point method[43] (Fig. 2). In short, this method iteratively minimizes (1) an objective function (negative motor improvement) and (2) constraint violations such as side-effect probabilities. Both conditions are related by a barrier function that is updated with each iteration. Finally, the optimizer converges when stopping

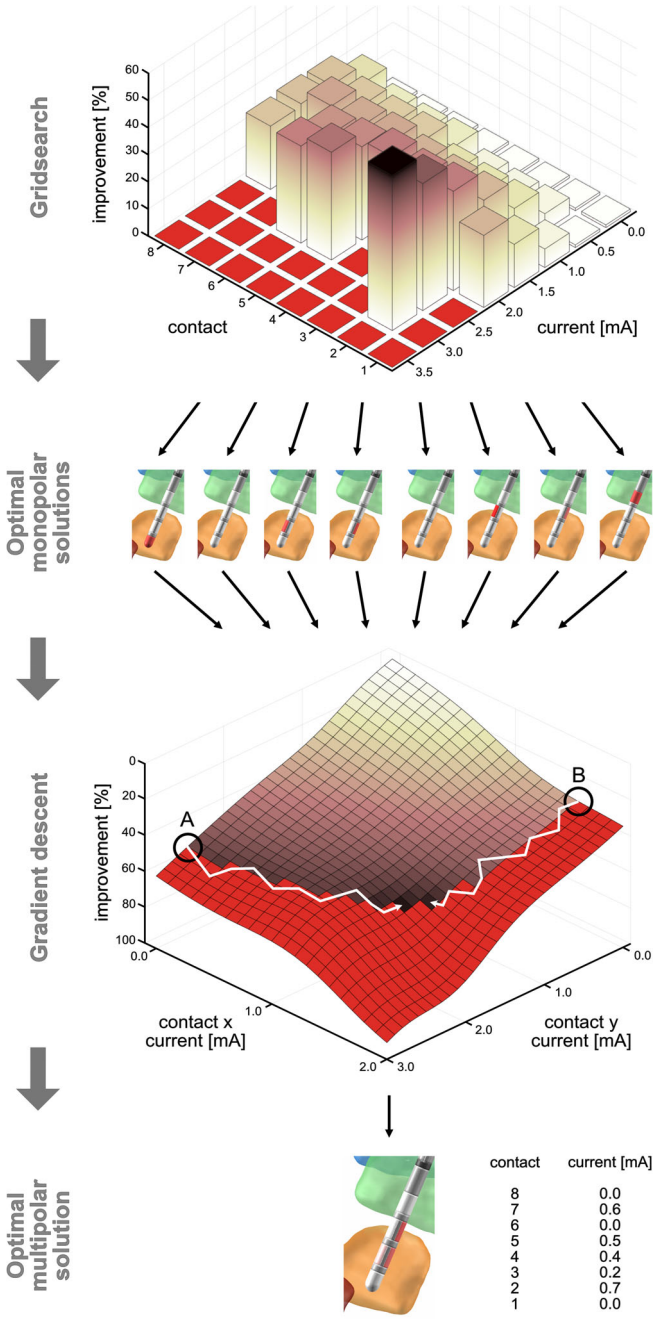

FIG. 2. Multistart optimization within the *StimFit* algorithm. First row: bar plot showing predicted motor improvements in respect to stimulation amplitudes at contacts 1 to 8. Settings with predicted side-effect probabilities exceeding the predefined threshold of 20% are shown in red and excluded from further analysis. Second row: optimal monopolar settings were identified for each contact and used as starting points for the optimizer. Third row: gradient descent optimization illustrated on two contacts x and y, starting at optimal monopolar settings A and B, respectively. Distribution of electric current was iteratively changed (white arrows) to find the optimal solution while avoiding settings with predicted side-effect probabilities greater than the predefined threshold of 20% (red areas). Both runs converged on approximately the same global minimum. Fourth row: final multicathode solution with greatest predicted motor improvement. Contacts were colored according to the distribution of electric current. [Color figure can be viewed at wileyonlinelibrary.com]

criteria such as minimum step sizes (step tolerance) or motor improvements (function tolerance) are fulfilled. In other words, the algorithm iteratively explores different combinations of stimulation settings to find the solution with optimal motor benefit, avoiding solutions with predicted side-effect probabilities greater than the predefined threshold. In addition, depending on the technical restrictions of the implanted DBS device, the algorithm allowed to define further constraints like minimum and maximum current per contact as well as maximum total current. Details of this algorithm are provided in Appendix S1, which also includes a description of measures implemented to reduce computational cost to maximize processing speed. The complete algorithm was condensed in a MATLAB-based graphical user interface and will be referred to as *StimFit* subsequently.

Validation of Automatically Derived Optimal Stimulation Settings

The *StimFit* algorithm was applied on all 19 patients from the test cohort. To test whether *StimFit* settings suggested by the algorithm were associated with superior clinical outcome, agreements between *StimFit* and the two empirical stimulation settings were calculated using Dice similarity coefficients for each pair of the three volumes of tissue activated (VTAs). VTAs were directly derived from E-fields by thresholding the norm at a vector magnitude of 0.2 V/mm.[6,44] Finally, differences in clinical outcomes between the two empirical settings were correlated with differences in their Dice coefficients with the automated settings. Intuitively, a high correlation in this analysis would imply that settings with stimulated regions similar to the ones suggested by the *StimFit* algorithm would be associated with better clinical improvements.

Results

The training cohort consisted of 612 stimulation settings in 31 patients with 46 DBS electrodes (16 unilateral cases) (Fig. 3A). Amplitudes were progressively tested from 0 to 5 mA in steps of 1 mA. Two patients were excluded due to suboptimal image quality. Tremor was present at baseline while testing 18 of 46 electrodes. Limiting side effects occurred in 127 of 167 tested contacts. If side effects occurred at amplitudes below 5 mA, it was assumed they would persist at higher amplitudes as well.

Within the fourfold cross-validation within the training sample, estimated motor improvements significantly correlated with observed improvements in $R = 0.57$ ($P < 10^{-10}$) (Fig. 4A). Median predicted side-effect probabilities in settings without observed side effects were 9% (IQR: 2%–37%) as opposed to 76% (IQR: 43%–93%) in settings where side effects were observed ($P < 10^{-10}$). The area under the ROC curve was 0.84 (Fig. 4B).

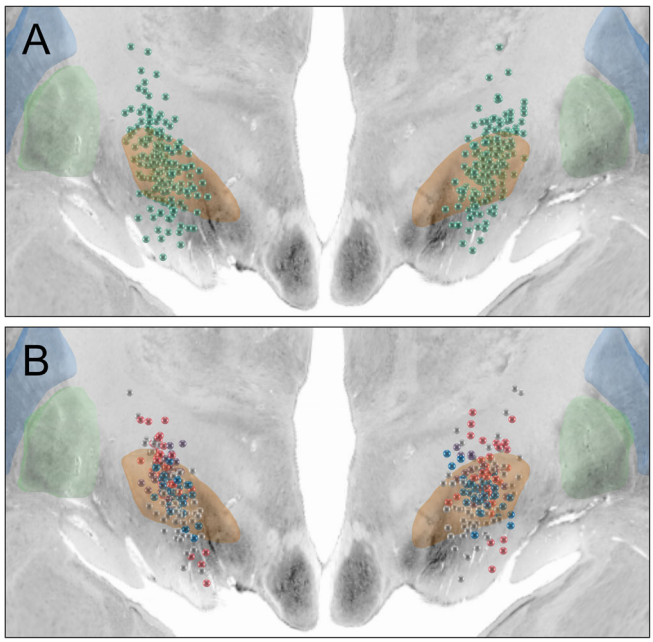

FIG. 3. Contact locations. Panels (**A**) and (**B**) showing the subthalamic nucleus (orange) as well as internal (light green) and external (light blue) parts of the globus pallidus. (**A**) Contact locations of the training cohort are shown as green spheres. (**B**) The contact locations of the test cohort with red and blue contacts active in settings 1 and 2, respectively, and purple and white contacts active in both or none of the settings. [Color figure can be viewed at wileyonlinelibrary.com]

The model was then tested on an independent cohort of 19 patients, each having received two different stimulation settings (1 and 2) (Fig. 3B). Motor improvements and side-effect probabilities of both settings were predicted using the vector models fit to data within the complete training data set. Because the overall goal of this project was to identify the optimal setting *within* one patient, model performance was assessed by its ability to estimate the difference in clinical outcomes between both settings. Therefore, differences in motor improvements between the two settings were calculated for both predicted and observed clinical outcomes. Doing so would automatically control for the "patient factor" (age, sex, disease duration, etc.). The model explained 28% of the variance in motor outcome differences ($R = 0.53$, $P < 10^{-3}$) (Fig. 4C). Despite these considerations about the "patient factor," it was still possible to significantly predict absolute outcomes across settings and patients, albeit to a lesser degree ($R = 0.36$, $P < 10^{-3}$).

Mapping grid-wise predictions of 2-mA cathodal stimulations at 125,000 locations in standard MNI space estimated an optimal motor improvement (averaging to 26%) for a contact position centered in the region of the dorsolateral STN border (Fig. 5; peak at

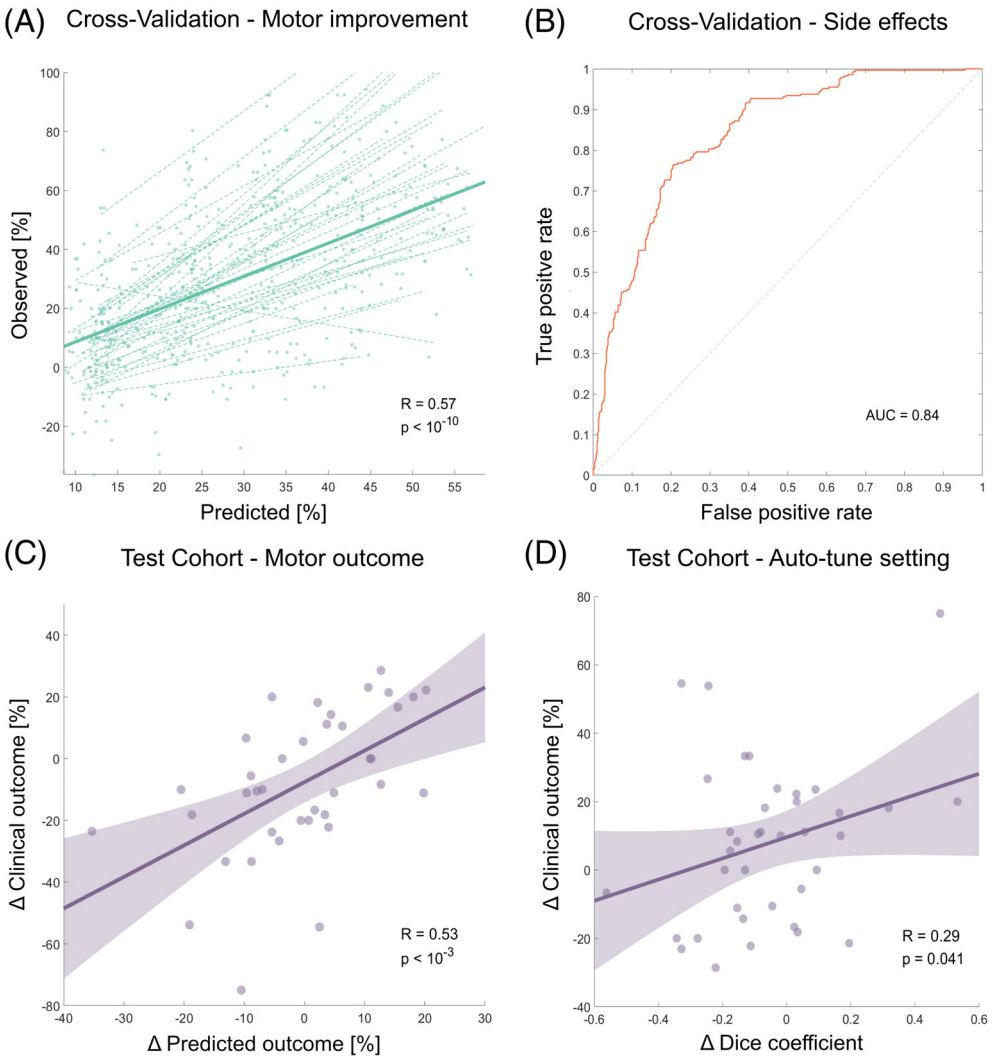

FIG. 4. Statistical results of the predictive model. (**A**) Linear models showing the relationship between predicted and observed motor improvements (fourfold cross-validation design) in the training cohort across all (thick green line) and within individual (dashed green lines) electrodes. (**B**) Receiver operating characteristic (ROC) curve (orange) of the side-effects model in the training cohort. (**C**) Relationship between predicted and observed differences in clinical outcomes (settings 1 vs. 2) in the test cohort. (**D**) Relationship between observed differences in clinical outcomes (settings 1 vs. 2) and spatial agreements between the two settings to the *StimFit* setting (quantified by Dice coefficients). [Color figure can be viewed at wileyonlinelibrary.com]

MNI coordinate $x = 13.5$, $y = -14.0$, $z = -3.6$ mm). Side-effect probabilities ranged from 8% to 13% and increased in regions of the ventral STN, substantia nigra pars reticulata, and internal capsule compared to lower side-effect probabilities in the dorsal STN, zona incerta, and ventral thalamic regions. Subanalyses of sweet spots for tremor and akinetic-rigid symptoms showed an anatomical separation of the two symptoms (Figure S2) with a maximum of (averaged) 23% improvement in akinetic-rigid symptoms when stimulating in the region of the dorsolateral border of the STN (peak at $x = 13.4$, $y = -14.2$, $z = -3.8$ mm) and optimal tremor improvement averaging at 45% in the zona incerta close to the ventral intermediate nucleus of the thalamus ($x = 14.2$, $y = -15.0$, $z = -2.1$ mm). Vector-field models validated in the previous sections were used as backbone models to identify optimal stimulation (*StimFit*) settings that would lead to optimal motor improvements while accounting for side effects.

StimFit settings were calculated for all patients from the test cohort. Agreements between *StimFit* and empirical settings were estimated using Dice coefficients between resulting VTAs. Greater spatial agreement between clinical stimulation settings and the ones suggested by *StimFit* setting was associated with better clinical improvement ($R = 0.29$, $P = 0.041$) (Fig. 4D). Electrode locations and *StimFit* settings for 3 representative patients (9, 11, and 18) are shown in Figure S1. Contact coordinates in MNI space as well as optimizer solutions of all patients are provided in Table S1.

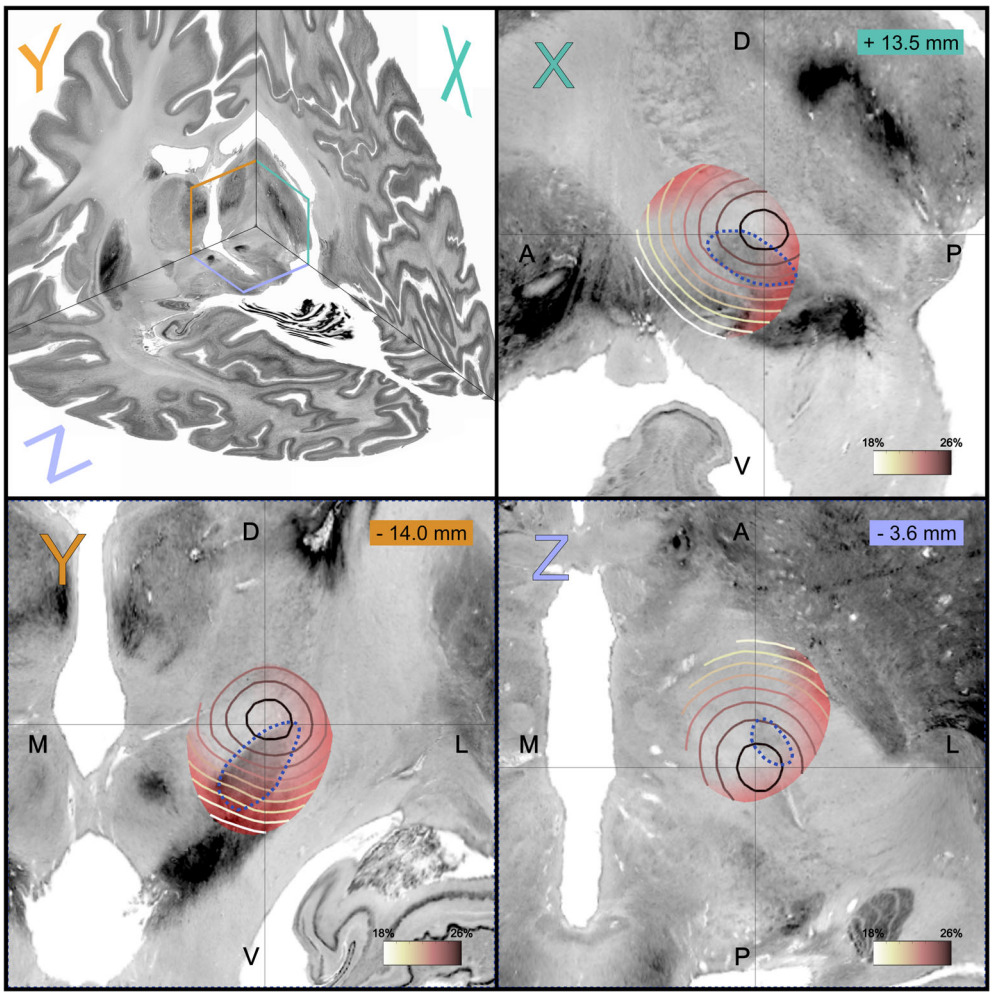

FIG. 5. Optimal stimulation sites (sweet-spot analysis). By "inverting" the predictive model in a brute-force manner, optimal stimulation sites (sweet spots) and regions with maximal probabilities to induce side effects (sour spots) could be calculated. Sagittal (top right), frontal (bottom left), and axial (bottom right) slices of the BigBrain Atlas 1 are shown at their intersection level with the peak coordinate of the sweet spot ($x = 13.5$, $y = -14.0$, $z = -3.6$). The right subthalamic nucleus is outlined by a dashed blue line. Maximum motor outcome (>26%) was predicted when the active contact was located within the area circled in black. Areas with increased side-effect probabilities are colored in shades of red. A, anterior; P, posterior; V, ventral; D, dorsal; L, lateral; M, medial. [Color figure can be viewed at wileyonlinelibrary.com]

Discussion

In this study we developed and validated a data-driven approach to automatically suggest STN-DBS stimulation parameters that would lead to maximal therapeutic benefit with a low risk of inducing side effects in patients with PD.

We did so in a three-step approach, first, by creating voxel-segment-based mixed models, each giving a prediction of stimulation effects as a function of prevalent E-field vector directions and magnitudes. This led to an ensemble model that could derive robust estimates of the overall effect induced by stimulation. We validated the approach in an independent test cohort of patients. Second, we applied hypothetical stimulations to the model to obtain an optimal stimulation sweet spot both for general motor improvement and for specific subsymptoms, as well as sour spots that would carry a high probability to induce side effects. Finally, we added a solver to the model that could automatically suggest stimulation parameters considering both therapeutic benefit and side-effect probabilities. We validated these automated suggestions retrospectively and concluded that parameter settings suggested by *StimFit* would indeed be associated with optimal clinical outcomes. Future prospective trials should further validate the model for clinical routine.

Vector-Field Model

Whereas many previous approaches to guide DBS parameter selection were based on visual,[15,19,45,46] kinematic,[32] or electrophysiological feedback,[47] this study proposes a fully automated algorithm, which suggests optimal stimulation settings based on neuroimaging data. The model underlying our approach is based on the properties of the E-field in the target area, which crucially considers

directionality of the voltage gradient. Directionality of the voltage distribution has impacted axonal activations in silico and in vivo and has been neglected by approaches that build on binary VTA models.[24,25]

Model Validation and Anatomical Implications

Results could validate an E-field-based modeling approach both quantitatively and anatomically. Model performance within the training cohort was comparable to the performance in a cross-center independent test cohort, indicating generalizability of the model.

In line with most recent studies, the sweet spot for optimal overall clinical improvement was situated at the dorsolateral border of the STN.[8-10,12,13,48] Symptom-specific sweet-spot analysis of the model showed optimal suppression of akinetic-rigid symptoms again in the dorsolateral region of the STN, whereas tremor suppression was greatest in the zona incerta close to the ventral intermediate nucleus of the thalamus. These findings are in line with accumulating evidence, suggesting that the dentato-rubro-thalamic tract might be a common target structure for tremor suppression across multiple underlying pathologies.[2,49-52] However, in the case of parkinsonian tremor, stimulating the STN proper might bear therapeutic effects as well.[53] Nonetheless, the symptom specificity related to different anatomical target structures indicates that individual symptomatology could influence the optimal contact selection.

Optimization Problem

Finding an optimal solution of a complex problem with multiple input variables and possible constraints is a typical engineering problem. (Non)linear programming algorithms allow to solve these types of problems in a time-efficient manner. To improve speed and efficacy in our approach, "monopolar reviews" were simulated first, and optimal monopolar solutions for all contacts were used as starting points for the optimizer, in parallel (see Appendix S1 and Fig. 2). This resembled the procedure of the clinical routine involved in DBS programming, in which monopolar settings are often explored first before even beginning to test the more complex multipolar settings.[54] Furthermore, this ensured that the optimizer would only suggest multicathode solutions when an additional clinical benefit was predicted compared to monopolar settings.

Other groups have used similar mathematical optimization strategies for automated DBS programming in the past. Anderson and colleagues applied linear programming to identify contacts that would maximize the stimulation of target structures and minimize the activation of regions of avoidance in silico.[14] Interestingly, this approach generalized well for electrodes of variable designs, including the Medtronic Sapiens electrodes (which with 32 contacts would be too complex to be manually programmed). Similarly, Vorwerk and colleagues demonstrated the use of constrained optimization algorithms to identify multicathode contact configurations leading to a maximum in silico activation of the ventral intermediate nucleus of the thalamus and minimal activation of surrounding, possibly side-effect-inducing thalamic nuclei.[17] In all of the five electrodes tested, the best clinical contacts were also assigned the maximum voltage by the algorithm. Using patient-specific anatomical data, Pena and colleagues demonstrated the use of particle-swarm optimization for optimization problems with multiple objectives.[16] This allowed to identify multicathode stimulation settings that would maximize activation of multiple target pathways although minimizing the activation of others. This might be of special interest considering the aforementioned strategy to engage multiple symptom-specific targets in PD but could also be of importance for optimization problems that simultaneously use multiple input modalities, as suggested in recent publications.[27,47]

Limitations

First, the assessment of monopolar review data, which have been used for training our model, has certain limitations. Those include a short wash-in period, imposing the risk of introducing bias toward short-term effects. Further, thresholding stimulation amplitudes at 5 mA (or permanent side effects) might introduce a potential ceiling bias because some effects might be observed only at higher amplitudes. Similarly, a step size of discretized amplitude increases (1 mA) may represent a certain sampling bias. In our opinion however, those disadvantages are outweighed by the benefits of standardized monopolar reviews. Those include an increased intraindividual outcome variability, unbiased selection of DBS settings, and evaluation of motor as well as side effects by the same rater at the same timepoint. Furthermore, limitations seem not to have impacted model performance to a degree that disenabled it to predict chronic UPDRS, Part III, improvements in an independent test cohort. Predictions of side effects, on the contrary, could not be evaluated in the test cohort because none of the chronic settings induced any permanent side effects. High-quality data sets of systematically assessed DBS-induced side effects are warranted to validate and potentially optimize our model.

Next, our training data consisted of a heterogenous collection of different electrode models that might potentially impact our analysis. However, this reflects the heterogeneity in clinical practice, and we therefore assume that this will increase the generalizability of our model.

This study uses a novel approach to predict outcome based on simulations of estimates of the E-field surrounding the electrodes. Different complexities of volume conductor models were used in the past, and in silico analyses have indicated that the choice of the model will impact simulated fiber activations.[55] Increasing the complexity of conductor models might improve accuracies in our approach but would also entail a

set of free parameters that need to be tuned due to ambiguities in biophysical tissue properties described in the literature.[28,29] We therefore chose to use a model with homogeneous tissue properties in template space using typical conductivity values from previous studies. Further work needs to be carried out to explore the potential benefit of increasing model complexity and native space simulations.

Further, in silico analyses of VTA-based predictive modeling approaches have shown to highly vary depending on their methodological details.[56] In this study we developed a novel method aiming at overcoming some of the limitations inherent to the concept of (binarized) VTA using a more nuanced, nonbinary concept in the form of E-field vectors. However, we do not provide evidence for the superiority of this choice. It is crucial to note that our choice of E-field vectors should not be interpreted as a disapproval of the VTA model but rather as an additional option to model DBS effects. Further in silico studies and head-to-head comparisons of different modeling approaches based on empirical multicenter data would be ideal to compare the utility of VTA versus E-field versus other modeling concepts.

Although agreement between empirical and model-based predictions of clinical improvements should be considered well ($R > 0.5$), similarities between StimFit and empirical settings (quantified as Dice coefficients) were only moderately correlated to clinical improvements ($R = 0.29$). We believe that, among others, the following reasons could be at play. First, Dice coefficients are a somewhat vague metric to assess similarities between settings. In other words, VTAs of different sizes and locations can lead to the same Dice coefficient, whereas stimulation effects may be different. Second, as discussed in this manuscript, the VTA itself as a predictor of stimulation effects inherits several limitations. Third, we are comparing parameter suggestions not to the optimal setting but to a sample drawn from all potential settings that are considered optimal in clinical routine. Settings other than the ones suggested by our model might therefore lead to comparable clinical effects. Therefore, the indirect validation of StimFit results needs to be interpreted with caution, and prospective evaluation of the model is required to fully assess the potential benefit of our guided programming approach. A prospective, randomized crossover noninferiority trial with this aim is currently ongoing (https://www.drks.de, study ID: DRKS00023115).

Conclusion

Our model was trained to suggest DBS parameters that would lead to optimal stimulation outcomes while accounting for stimulation-induced side effects. The model was validated by cross-validating within a training cohort and by predicting motor improvement in an independent test cohort. A clinical trial to prospectively validate the model is currently ongoing. In the future, our approach might help to guide DBS programming and could allow translation of scientific results from bench to bedside.

Acknowledgments: We thank Bassam Al-Fatly and Johannes Achtzehn for the fruitful and encouraging discussions.

Data Availability Statement

The data that support the findings of this study are available from the corresponding author upon reasonable request.

References

1. Krack P, Batir A, Van Blercom N, et al. Five-year follow-up of bilateral stimulation of the subthalamic nucleus in advanced Parkinson's disease. N Engl J Med 2003;349:1925–1934.
2. Al-Fatly B, Ewert S, Kubler D, Kroneberg D, Horn A, Kuhn AA. Connectivity profile of thalamic deep brain stimulation to effectively treat essential tremor. Brain 2019;142:3086–3098.
3. Baldermann JC, Melzer C, Zapf A, et al. Connectivity profile predictive of effective deep brain stimulation in obsessive-compulsive disorder. Biol Psychiatry 2019;85(9):735–743. https://doi.org/10.1016/j.biopsych.2018.12.019.
4. Dembek TA, Barbe MT, Astrom M, et al. Probabilistic mapping of deep brain stimulation effects in essential tremor. NeuroImage Clin 2017;13:164–173.
5. Dembek TA, Roediger J, Horn A, et al. Probabilistic sweet spots predict motor outcome for deep brain stimulation in Parkinson disease. Ann Neurol 2019;86:527–538. https://doi.org/10.1002/ana.25567
6. Horn A, Reich M, Vorwerk J, et al. Connectivity predicts deep brain stimulation outcome in Parkinson disease. Ann Neurol 2017;82:67–78.
7. Reich MM, Horn A, Lange F, et al. Probabilistic mapping of the antidystonic effect of pallidal neurostimulation: a multicentre imaging study. Brain. 2019;142:1386–1398. https://doi.org/10.1093/brain/awz046
8. Akram H, Sotiropoulos SN, Jbabdi S, et al. Subthalamic deep brain stimulation sweet spots and hyperdirect cortical connectivity in Parkinson's disease. Neuroimage 2017;158:332–345.
9. Bot M, Schuurman PR, Odekerken VJJ, et al. Deep brain stimulation for Parkinson's disease: defining the optimal location within the subthalamic nucleus. J Neurol Neurosurg Psychiatry 2018;89:493–498.
10. Horn A. The impact of modern-day neuroimaging on the field of deep brain stimulation. Curr Opin Neurol 2019;32:511–520.
11. Horn A, Fox MD. Opportunities of connectomic neuromodulation. Neuroimage 2020;221:117180
12. Boutet A, Germann J, Gwun D, et al. Sign-specific stimulation 'hot' and 'cold' spots in Parkinson's disease validated with machine learning. Brain Commun 2021;3:fcab027
13. Dembek TA, Roediger J, Horn A, et al. Probabilistic sweet spots predict motor outcome for deep brain stimulation in Parkinson disease. Ann Neurol 2019;86:527–538.
14. Anderson DN, Osting B, Vorwerk J, Dorval AD, Butson CR. Optimized programming algorithm for cylindrical and directional deep brain stimulation electrodes. J Neural Eng 2018;15:026005
15. Frankemolle AM, Wu J, Noecker AM, et al. Reversing cognitive-motor impairments in Parkinson's disease patients using a computational modelling approach to deep brain stimulation programming. Brain 2010;133:746–761.
16. Pena E, Zhang S, Patriat R, et al. Multi-objective particle swarm optimization for postoperative deep brain stimulation targeting of subthalamic nucleus pathways. J Neural Eng 2018;15:066020
17. Vorwerk J, Brock AA, Anderson DN, Rolston JD, Butson CR. A retrospective evaluation of automated optimization of deep brain stimulation parameters. J Neural Eng 2019;16:064002

18. Xiao Y, Pena E, Johnson MD. Theoretical optimization of stimulation strategies for a directionally segmented deep brain stimulation electrode Array. IEEE Trans Biomed Eng 2016;63:359–371.
19. Butson CR, Noecker AM, Maks CB, McIntyre CC. StimExplorer: deep brain stimulation parameter selection software system. Acta Neurochir Suppl 2007;97:569–574.
20. Timmermann L, Jain R, Chen L, et al. 134 VANTAGE trial: three-year outcomes of a prospective, multicenter trial evaluating deep brain stimulation with a new multiple-source, constant-current rechargeable system in Parkinson disease. Neurosurgery 2016;63(Suppl 1):155
21. Bour LJ, Lourens MA, Verhagen R, et al. Directional recording of subthalamic spectral power densities in Parkinson's disease and the effect of steering deep brain stimulation. Brain Stimul 2015;8:730–741.
22. Petersen MV, Mlakar J, Haber SN, et al. Holographic reconstruction of axonal pathways in the human brain. Neuron 2019;104: 1056–1064.e3.
23. Anderson CJ, Anderson DN, Pulst SM, Butson CR, Dorval AD. Neural selectivity, efficiency, and dose equivalence in deep brain stimulation through pulse width tuning and segmented electrodes. Brain Stimul 2020;13:1040–1050.
24. Anderson DN, Duffley G, Vorwerk J, Dorval AD, Butson CR. Anodic stimulation misunderstood: preferential activation of fiber orientations with anodic waveforms in deep brain stimulation. J Neural Eng 2019;16:016026
25. Lehto LJ, Slopsema JP, Johnson MD, et al. Orientation selective deep brain stimulation. J Neural Eng 2017;14:016016
26. Gunalan K, Chaturvedi A, Howell B, et al. Creating and parameterizing patient-specific deep brain stimulation pathway-activation models using the hyperdirect pathway as an example. PLoS One 2017;12:e0176132
27. Howell B, Isbaine F, Willie JT, et al. Image-based biophysical modeling predicts cortical potentials evoked with subthalamic deep brain stimulation. Brain Stimul 2021;14:549–563.
28. McCann H, Pisano G, Beltrachini L. Variation in reported human head tissue electrical conductivity values. Brain Topogr 2019;32:825–858.
29. McCann H, Pisano G, Beltrachini L. Correction to: variation in reported human head tissue electrical conductivity values. Brain Topogr 2021;34:110–115.
30. Jakobs M, Fomenko A, Lozano AM, Kiening KL. Cellular, molecular, and clinical mechanisms of action of deep brain stimulation—a systematic review on established indications and outlook on future developments. EMBO Mol Med 2019;11. https://doi.org/10.15252/emmm.201809575
31. Dembek TA, Reker P, Visser-Vandewalle V, et al. Directional DBS increases side-effect thresholds-a prospective, double-blind trial. Mov Disord 2017;32:1380–1388.
32. Wenzel GR, Roediger J, Brucke C, et al. CLOVER-DBS: algorithm-guided deep brain stimulation-programming based on external sensor feedback evaluated in a prospective, randomized, crossover, double-blind, two-center study. J Parkinsons Dis 2021; 11(4):1887–1899.
33. Horn A, Kuhn AA. Lead-DBS: a toolbox for deep brain stimulation electrode localizations and visualizations. Neuroimage 2015;107:127–135.
34. Horn A, Li N, Dembek TA, et al. Lead-DBS v2: towards a comprehensive pipeline for deep brain stimulation imaging. Neuroimage 2019;184:293–316.
35. Avants BB, Epstein CL, Grossman M, Gee JC. Symmetric diffeomorphic image registration with cross-correlation: evaluating automated labeling of elderly and neurodegenerative brain. Med Image Anal 2008;12:26–41.
36. Hellerbach A, Dembek TA, Hoevels M, et al. DiODe: directional orientation detection of segmented deep brain stimulation leads: a sequential algorithm based on CT imaging. Stereotact Funct Neurosurg 2018;96:335–341.
37. Husch A, Petersen MV, Gemmar P, Goncalves J, Hertel F. PaCER - a fully automated method for electrode trajectory and contact reconstruction in deep brain stimulation. NeuroImage Clin 2018;17:80–89.
38. Fang Q. Iso2Mesh. 2021. https://github.com/fangq/iso2mesh
39. Si H. TetGen, a delaunay-based quality tetrahedral mesh generator. ACM Trans Math Software 2015;42:1–36.
40. Oostenveld R, Fries P, Maris E, Schoffelen JM. FieldTrip: open source software for advanced analysis of MEG, EEG, and invasive electrophysiological data. Comput Intell Neurosci 2011;2011:156869
41. Vorwerk J, Cho JH, Rampp S, Hamer H, Knosche TR, Wolters CH. A guideline for head volume conductor modeling in EEG and MEG. Neuroimage 2014;100:590–607.
42. Baniasadi M, Proverbio D, Goncalves J, Hertel F, Husch A. FastField: an open-source toolbox for efficient approximation of deep brain stimulation electric fields. Neuroimage 2020;223:117330
43. Byrd R, Gilbert J, Nocedal J. A trust region method based on interior point techniques for nonlinear programming. Math Program 2000;89:149–185.
44. Astrom M, Diczfalusy E, Martens H, Wardell K. Relationship between neural activation and electric field distribution during deep brain stimulation. IEEE Trans Biomed Eng 2015;62:664–672.
45. Butson CR, Tamm G, Jain S, Fogal T, Kruger J. Evaluation of interactive visualization on mobile computing platforms for selection of deep brain stimulation parameters. IEEE Trans Vis Comput Graph 2013;19:108–117.
46. Pavese N, Tai YF, Yousif N, Nandi D, Bain PG. Traditional trial and error versus Neuroanatomic 3-dimensional image software-assisted deep brain stimulation programming in patients with Parkinson disease. World Neurosurg 2020;134:e98–e102.
47. Connolly MJ, Cole ER, Isbaine F, et al. Multi-objective data-driven optimization for improving deep brain stimulation in Parkinson's disease. J Neural Eng 2021;18. https://doi.org/10.1088/1741-2552/abf8ca
48. Caire F, Ranoux D, Guehl D, Burbaud P, Cuny E. A systematic review of studies on anatomical position of electrode contacts used for chronic subthalamic stimulation in Parkinson's disease. Acta Neurochir 2013;155:1647–1654; discussion 54.
49. Coenen VA, Sajonz B, Prokop T, et al. The dentato-rubro-thalamic tract as the potential common deep brain stimulation target for tremor of various origin: an observational case series. Acta Neurochir 2020;162:1053–1066.
50. Listik C, Santiago N, Reis PR, et al. Targeting the hot spot in a patient with essential tremor and Parkinson's disease: tractography matters. Clin Neurol Neurosurg 2018;174:230–232.
51. Abdulbaki A, Kaufmann J, Galazky I, Buentjen L, Voges J. Neuromodulation of the subthalamic nucleus in Parkinson's disease: the effect of fiber tract stimulation on tremor control. Acta Neurochir 2021;163:185–195.
52. Dembek TA, Petry-Schmelzer JN, Reker P, et al. PSA and VIM DBS efficiency in essential tremor depends on distance to the dentatorubrothalamic tract. NeuroImage Clin 2020;26:102235
53. Helmich RC, Hallett M, Deuschl G, Toni I, Bloem BR. Cerebral causes and consequences of parkinsonian resting tremor: a tale of two circuits? Brain 2012;135:3206–3226.
54. Soh D, Maciel R, Algarni M, et al. Flexible vs. standard subthalamic stimulation in Parkinson disease: a double-blind proof-of-concept cross-over trial. Parkinsonism Relat Disord 2021;89:93–97.
55. Howell B, McIntyre CC. Analyzing the tradeoff between electrical complexity and accuracy in patient-specific computational models of deep brain stimulation. J Neural Eng 2016;13:036023
56. Dembek TA, Baldermann JC, Petry-Schmelzer JN, et al. Sweetspot mapping in deep brain stimulation: strengths and limitations of current approaches. Neuromodulation 2021;

Supporting Data

Additional Supporting Information may be found in the online version of this article at the publisher's web-site.